



Long-term analysis of clear-sky new particle formation events and non-events in Hyytiälä

Lubna Dada¹, Pauli Paasonen¹, Tuomo Nieminen^{1,2}, Stephany Buenrostro Mazon¹, Jenni Kontkanen¹, Otso Peräkylä¹, Tareq Hussein^{1,4}, Tuukka Petäjä¹, Veli-Matti Kerminen¹, Jaana Bäck³, and Markku Kulmala¹

¹Department of Physics, University of Helsinki, P.O. Box 64, FIN-00014 Helsinki, Finland

²Department of Applied Physics, University of Eastern Finland, P.O. Box 1627, FI-70211 Kuopio, Finland

³Department of Forest Sciences, University of Helsinki, P.O. Box 27, FIN-00014 Helsinki, Finland

⁴Department of Physics, the University of Jordan, Amman 11942, Jordan

Correspondence to: Lubna Dada (lubna.dada@helsinki.fi)

Abstract. New particle formation (NPF) events have been observed all around the world and are known to be a major source of atmospheric aerosol particles. Here we combine 20 years of observations in a boreal forest at the SMEAR II station (Station for Measuring Ecosystem-Atmosphere Relations) in Hyytiälä, Finland, by utilizing previously accumulated knowledge, and by focusing on clear-sky (non-cloudy) conditions. We first investigated the effect of cloudiness on NPF and then compared the NPF event and non-event days during clear-sky conditions. In this comparison we considered, for example, the effects of calculated particle formation rates, condensation sink, trace gas concentrations and various meteorological quantities. The formation rate of 1.5 nm particles was calculated by using proxies for gaseous sulfuric acid and oxidized products of low volatile organic compounds. As expected, our results indicate an increase in the frequency of NPF events under clear-sky conditions. Also, focusing on clear-sky conditions enabled us to find a clear separation of many variables related to NPF. For instance, oxidized organic vapors showed higher concentration during the clear-sky NPF event days, whereas the condensation sink (CS) and some trace gases had higher concentrations during the non-event days. The calculated formation rate of 3 nm particles showed a notable difference between the NPF event and non-event days during clear-sky conditions, especially in winter and spring. For spring time, we are able to find a threshold value for the combined values of ambient temperature and CS, above which practically no clear-sky NPF event could be observed. Finally, we present a probability distribution for the frequency of NPF events at a specific CS and temperature.

Keywords: Boreal forest, formation rate, atmospheric aerosols, aerosol dynamics, condensation sink, cloudiness parameter



1 Introduction

The effects of atmospheric aerosol particles on the climate system, human health and environmental interactions have raised the interest in various phenomena associated with the formation, growth and loss of these particles (Pöschl, 2005; Seinfeld and Pandis, 2012; Apte et al., 2015). While primary emissions are a very important source of atmospheric aerosol particles, especially in terms of the aerosol mass loading, the particle number concentration is greatly affected by atmospheric new particle formation (NPF). During the last couple of decades, NPF has been observed to take place almost all over the world (Kulmala et al., 2004a; Zhang et al., 2011; Kontkanen et al., 2015; Bianchi et al., 2016). Atmospheric NPF is thought to be the dominant source of the total particle number concentration, and a major source of cloud condensation nuclei, in the global troposphere (Merikanto et al., 2009; Yu et al., 2010; Kerminen et al., 2012; Kulmala et al., 2016).

Understanding the NPF phenomenon requires understanding the precursors and pathways involved under different atmospheric conditions. For instance, high concentrations of low-volatility vapors result in a higher probability for NPF (Nieminen et al., 2015), whereas a high relative humidity and condensation sink tend to suppress NPF (Hyvönen et al., 2005; Nieminen et al., 2014). Recent laboratory experiments have shown the importance of sulfuric acid and low-volatile oxidized organic vapors on NPF (Metzger et al., 2010; Kirkby et al., 2011; Petäjä et al., 2011; Kulmala et al., 2013; Ehn et al., 2014; Riccobono et al., 2014). Additionally, atmospheric observations confirm the importance of these precursor vapors in the initial steps of NPF and in the further growth of newly-formed particles (Kulmala et al., 1998; Smith et al., 2005; Kerminen et al., 2010; Paasonen et al., 2010; Ahlm et al., 2012; Bzdek et al., 2014; Nieminen et al., 2014; Vakkari et al., 2015).

Amongst the studies investigating the role of different variables in causing, enhancing or preventing new particle formation (Hyvönen et al., 2005; Nieminen et al., 2014), Baranizadeh et al. (2014) studied the effect of cloudiness on NPF events in Hyytiälä, a boreal forest environment in Southern Finland. That study concluded, in agreement with some other studies, the role of clouds in attenuating and interrupting NPF events (Sogacheva et al., 2008; Boulon et al., 2010; Baranizadeh et al., 2014; Nieminen et al., 2015). In this study, we eliminate one variable that limits NPF (cloudiness), in order to provide a better insight into the other parameters related to NPF rate and its probability. Based on 20-years of observations and data analysis for the SMEAR II station in Hyytiälä, we aim to i) quantify the effect of cloudiness on new particle formation frequency, ii) characterize the differences between NPF event and non-event days during clear-sky conditions, iii) find out the connection between nucleating precursor vapors and new particle formation rates and iv) formulate an equation that predicts whether NPF occurs or not during clear-sky conditions.



68 **2 Materials and Methods**

69 **2.1 Measurements**

70

71 The data used for the analysis in this study is from the University of Helsinki SMEAR (Station for Measurement of
72 Ecosystem –Atmosphere Relations) II station (Hari and Kulmala, 2005). The station provides long-term continuous
73 comprehensive measurements of quantities describing the atmospheric-forest-ecosystem interactions. The SMEAR II
74 station is located in the boreal forest in Hyytiälä, southern Finland (61°51N', 24°17E', 181 m a.s.l.), 220 km NW of
75 Helsinki. Tampere (200,000 inhabitants) is the largest city nearest to the station and is located 60 km SW of the site.
76 Being far from major human activities and surrounded by a homogenous scots pine belt, Hyytiälä is considered a rural
77 background site due to the low levels of air pollutants (Asmi et al., 2011). A more detailed overview of the measurements
78 at the station can be found in Hari and Kulmala (2005) and Nieminen et al. (2014).

79

80 In this study, data analysis is based on four types of measurements: (i) aerosol particle number size distributions, (ii)
81 concentration of the trace gases (CO, NO, NO₂, NO_x, SO₂ and O₃), (iii) meteorological parameters (solar radiation,
82 temperature and relative humidity), and (iv) precursor vapor concentrations from previously-developed proxies. The
83 collection of data started in January 1996. Trace gas concentrations are measured at 6 different heights on a 74-m-high
84 mast (extended to 126 m in summer 2010). Gas concentrations used in this study are collected from the middle level on
85 the mast above the forest (at 16.8 m).

86 **2.1.1 Particle number size distributions**

87

88 The aerosol number concentration size distributions were measured with a twin-DMPS (Differential Mobility Particle
89 Sizer) system (Aalto et al., 2001) for the size ranges 3-500 nm until year 2004 and 3-1000 nm from 2005 onwards. The
90 data measured was used to classify days as NPF events and non-events following the method proposed by Dal Maso et
91 al. (2005). The size distributions obtained from the DMPS measurements were used to calculate the condensation sink,
92 CS, which is equal to the rate at which non-volatile vapors condense onto a pre-existing aerosol particle population
93 (Kulmala et al., 2012).

94 **2.1.2 Trace Gases**

95

96 The CO concentration is measured with one infrared light absorption analyzer (API 300EU, Teledyne Monitor Labs,
97 Englewood, CO, USA). The NO and NO_x concentrations are monitored with a chemiluminescence analyzer (TEI 42C
98 TL, Thermo Fisher Scientific, Waltham, MA, USA). The NO₂ concentration is calculated from the difference NO_x–NO.
99 The detection limit is about 0.05 ppb. SO₂ measurements are made through a UV-fluorescence analyzer (TEI 43 CTL,
100 Thermo Fisher Scientific, Waltham, MA, USA) that has a detection limit of 0.1 ppb. The O₃ concentration is measured
101 with an UV light absorption analyzer (TEI 49C, Thermo Fisher Scientific, Waltham, MA, USA) that has a detection limit
102 of about 1 ppb. The data for trace gases are available as 30-minute arithmetic means.



2.1.3 Radiation

Solar radiation in the wavelengths of UV-B (280 – 320nm) and global radiation (0.30 - 4.8 μm) are monitored using pyranometers (SL 501A UVB, Solar Light, Philadelphia, PA, USA; Reeman TP 3, Astrodata, Tõravere, Tartumaa, Estonia until June 2008, and Middleton Solar SK08, Middleton Solar, Yarraville, Australia since June 2008) above the forest at 18 m. The air temperature is measured with 4-wired PT-100 sensors, and the relative humidity (in percent) is measured with relative humidity sensors (Rotronic Hygromet MP102H with Hygroclip HC2-S3, Rotronic AG, Bassersdorf, Switzerland). These data are provided as 30-minute averages.

2.1.4 Sulfuric Acid and Oxidized Organics Proxies

The gaseous sulfuric acid concentration is estimated from a pseudo-steady-state-approximation proxy developed by Petäjä et al. (2009). This proxy takes into consideration the sulfuric acid source and sink terms as

$$[\text{H}_2\text{SO}_4]_{\text{proxy}} = k \cdot \frac{[\text{SO}_2] \cdot \text{UVB}}{\text{CS}} (1).$$

Here, UVB (W m^{-2}) is the fraction of the UV radiation reaching earth after being screened by ozone (280 – 320 nm) and the coefficient k ($\text{m}^2 \text{W}^{-1} \text{s}^{-1}$) is obtained from the comparison of the proxy concentration to the available measured H_2SO_4 data, and has a median value of $9.9 \times 10^{-7} \text{ m}^2 \text{W}^{-1} \text{s}^{-1}$.

The concentration of monoterpene oxidation products, called oxidized organic compounds (OxOrg) here, is estimated using a proxy developed by Kontkanen et al. (2016). This proxy is calculated by using the concentrations of different oxidants (the measured ozone concentration $[\text{O}_3]$ and parameterizations for the hydroxyl and nitrate radical concentration, $[\text{OH}]$ and $[\text{NO}_3]$, respectively) and their reaction rates, k_i , with the monoterpenes. The MT_{proxy} is calculated by taking into account the effect of temperature-driven emissions, mixing of the boundary layer and the oxidation of monoterpenes, (Kontkanen et al., 2016).

$$[\text{OxOrg}]_{\text{proxy}} = \frac{(k_{\text{OH}} + \text{MT}[\text{OH}] + k_{\text{O}_3} + \text{MT}[\text{O}_3] + k_{\text{NO}_3} + \text{MT}[\text{NO}_3]) \cdot \text{MT}_{\text{proxy}}}{\text{CS}} (2).$$

2.1.5 Backward Air-mass Trajectories

Air mass trajectories were calculated using Hybrid Single-Particle Lagrangian Integrated Trajectory (HYSPPLIT_4) Model at 96-hour backward trajectories at 100, 250 and 500 m arrival heights once per hour. Free access to transport model is developed and provided by NOAA (<http://www.ready.noaa.gov/HYSPLIT.php>). Input meteorological data required for the model were collected from GDAS (Global Data Assimilation System) archives.



139 2.2 Data Analysis

140 2.2.1 New Particle Formation Events

141

142 Formation of new aerosol particles in Hyytiälä is typically observed in the time window of several hours around noon,
 143 while this phenomenon seems to be rare during nighttime (Junninen et al., 2008;Buenrostro Mazon et al., 2016).
 144 Accordingly, aerosol number size distributions data from the DMPS measurements at around this time window are used
 145 for classifying individual days as new particle formation event or non-event days. The classification follows the guidelines
 146 presented by Kulmala et al. (2012), and the procedure presented in Dal Maso et al. (2005).

147

148 2.2.2 Selecting Non-cloudy Days

149

150 Cloudiness parameter (P) is the ratio of measured global radiation (R_d) divided by the theoretical global irradiance (R_g):

151

$$152 \quad P = \frac{R_d}{R_g} \quad (3)$$

153 The theoretical maximum of global radiation (R_g) is calculated by taking into consideration the latitude of the
 154 measurement station and the seasonal solar cycle. While a complete cloud coverage is classified as $P < 0.3$, a clear-sky is
 155 classified as $P > 0.7$ (Perez et al., 1990;Sogacheva et al., 2008;Sánchez et al., 2012). Accordingly, in this work the days
 156 were classified as cloudy or clear-sky days based on the median value of P during 9:00-12:00 each day, corresponding to
 157 the time window for new particle formation. Clear-sky days were those with a median of $P > 0.7$ between 9:00 and 12:00
 158 and are the focus of this study.

159

160 2.2.3 Particle Formation Rates

161

162 The formation rate of nucleation mode particles ($J_{3,C}$, particle diameter > 3 nm) was calculated based on the method
 163 suggested by Kerminen and Kulmala's equation (Kerminen and Kulmala, 2002). This quantity is a function of the
 164 calculated formation rate of 1.5 nm sized particles ($J_{1.5,C}$), their growth rate (GR) and the condensation sink (CS):

$$165 \quad J_{3,C} = J_{1.5,C} \exp \left(-\gamma \frac{CS'}{GR_{1.5-3}} \left(\frac{1}{1.5} - \frac{1}{3} \right) \right), \quad (4)$$

166 where γ is a coefficient with an approximate value of $0.23 \text{ m}^3 \text{ nm}^2 \text{ s}^{-1}$. The value of $J_{1.5,C}$ was calculated by assuming
 167 heteromolecular nucleation between SA and OxOrg as follows:

168

$$169 \quad J_{1.5,C} = K_{\text{het}} [\text{H}_2\text{SO}_4]_{\text{proxy}} [\text{OxOrg}]_{\text{proxy}}, \quad (5)$$

170

171 The heterogeneous nucleation coefficient used in Equation 5 is the median estimated coefficient for Hyytiälä scaled from
 172 Paasonen et al. (2010): $K_{\text{het}} = 9.2 \times 10^{-14} \text{ cm}^3 \text{ s}^{-1}$. The scaling was made in order to fit the current data. The median value
 173 of $[\text{OxOrg}]$ during the event days in April and May was found to be $1.3 \times 10^8 \text{ cm}^{-3}$ (Paasonen et al., 2010), whereas the
 174 improved median value of $[\text{OxOrg}]$ by Kontkanen et al. (2016) is $1.6 \times 10^7 \text{ cm}^{-3}$. The scaling factor is the ratio between



175 new and original [OxOrg] (0.1194); Accordingly, while the value of K_{het} from Paasonen et al. (2010) is $1.1 \times 10^{-13} \text{ cm}^3 \text{ s}^{-1}$,
176 ¹, after the scaling by 0.1194 we obtain the revised $K_{het} = 9.2 \times 10^{-14} \text{ cm}^3 \text{ s}^{-1}$.
177

178 The particle growth rate over the particle diameter range of 1.5–3 nm was calculated by taking into account the size of
179 the condensing vapor molecule size and the thermal speed of the particle (Nieminen et al., 2010). The growth rates (1.5
180 – 3 nm) were calculated as 30-minute averages and as the sum of the growth rates due to the sulfuric acid (SA) vapor and
181 OxOrg vapor condensation. The density of the particle was assumed to be constant (1440 kg/m^3). For SA, we first
182 determined the SA concentration needed to make the particles grow at the rate of 1 nm/h by taking into account the mass
183 of hydrated SA at the present RH and its density (Kurtén et al., 2007). Then, we calculated the GR of the particles due to
184 SA condensation by using the SA proxy concentration. The same method was used for GR due to OxOrg condensation,
185 where the vapor density was assumed to be 1200 kg/m^3 (Kannosto et al., 2008; Hallquist et al., 2009). Similarly, the GR
186 due to OxOrg was calculated by using OxOrg proxy concentrations divided by the concentration needed for 1 nm/h GR.
187



3 Results and discussion

3.1 Effect of Cloudiness on NPF

We studied NPF events as a function of cloudiness. Figure 1a shows the fraction of event, non-event and undefined days as a function of cloudiness parameter. We can see that clear-sky conditions favor the occurrence of NPF: the less clouds there were, the higher was the fraction of NPF event days. For instance, for days with the cloudiness parameter of 0.3 or less, the fraction of event days was less than 0.1 of the total classified days. However, the fraction of NPF event days reached a maximum of around 0.55 during complete clear-sky conditions ($P > 0.7$), with 877 days classified as NPF events and only 229 as non-events. The pattern found in Figure 1a follows from the fact that radiation is essential for NPF as these events occur mainly during daylight hours (Kulmala et al., 2004b). NPF is favored under abundant radiation conditions, since sulfuric acid, which is the main component of freshly formed particles, is mainly formed photochemically (Petäjä et al., 2009). The fraction of undefined days, however, remained constant regardless of cloudiness conditions.

In Figure 1b we show the medians and percentiles of cloudiness parameters during the time window 9:00-12:00. As expected, NPF events tended to occur preferentially on the days having less clouds. On the NPF event days, the median cloudiness parameter during the time window 9:00-12:00 was found to be 0.75, while the non-event days were characterized by lower values of this parameter (a median of around 0.25). Also, 75% of the NPF event days were found to have a cloudiness parameter larger than 0.5. Therefore, the fact that radiation favors NPF to occur is emphasized and correspondingly cloud cover decreases the probability of NPF. Undefined days were observed under cloudiness conditions that fell between those for NPF events and non-events. Undefined days can be interrupted NPF events or unclassified plumes of small particles due to pollution (Buenrostro Mazon et al., 2009). The interruption of a NPF event can be due to a change in the measured air mass, or due to attenuation of solar radiation caused by the appearance of a cloud during the event. In order to find out clear results and conclusions, we will focus on comparison between NPF events and non-events in following sections.

The monthly variation of daily median cloudiness parameter within the time window of 9:00-12:00 during the classified days is shown in Figure 2. While spring showed the best separation between the events and non-events in terms of the cloudiness parameter, the separation became weaker during the summer and specifically for June and July. Taken together, Figures 1 and 2 emphasize the observation that the presence of clouds decreases the probability of NPF events.

3.2 General Character of NPF on clear-sky days

Upon visualizing the cloudiness conditions during events and non-events, we chose a fixed constraint for clear-sky conditions ($P > 0.7$) during the time window of NPF (9:00-12:00) and will next focus on other parameters that distinguish NPF events from non-events.



The monthly distribution of the event fraction on clear-sky days appeared as double peaks in spring and autumn, with spring having a higher fraction of events (Figure 3a). The minimum fraction of NPF events was recorded in December. The fraction of non-event days peaked during winter with another peak in summer. It is important to note the annual variation of the number of NPF events during the years 1996-2015. However, this variation did not show any specific trend of frequency (Figure 3b), which is in agreement with previous statistics reported from studies that did not consider clear-sky classification (Nieminen et al., 2014).

3.2.1 Backward air mass trajectories during clear-sky NPF events and non-events

The springtime medians and percentiles of air-mass trajectories arriving at Hyytiälä during the NPF events and non-events were calculated 96 hours backward in time at the 100-m, 250-m and 500-m arrival heights for the years 1996-2015. The trajectories arriving at Hyytiälä at these three heights were quite similar, and those arriving at the 500-m height are shown in Figure 4. Medians and percentiles of the routes were calculated by taking the median of the trajectories at every half hour for spring time NPF event days and non-event days separately; spring time is chosen as it is the peak time of NPF. During the NPF event days, the measured air masses were found to originate mainly from the north and to pass over Scandinavia before arriving to Hyytiälä. Similar to previously reported results, air masses arriving from the north and north-west directions result in clean air with low pollutant (particulate matter and trace gas) concentrations (Nieminen et al., 2015). On the other hand, during NPF non-event days air masses originate from more polluted areas in Europe and Russia, resulting in elevated levels of condensation sink and other air pollutants in Hyytiälä, as reported by previous studies (Sogacheva et al., 2005).

3.2.2 Influences of CS, meteorological parameters and trace gases

In Figure 5a we present the monthly variation of condensation sink during NPF events and non-events under daytime clear-sky conditions. NPF events tended to be favored by low values of CS throughout the year. In all months, except during summer, the 75th percentile of the event day values of CS was lower than the 25th percentile of the non-event day values of CS. On the NPF event days, CS had its maximum in summer, which might be one of the main reasons for the local minimum in the NPF event frequency during the summer months (Figure 3a). However, the monthly cycle of CS on non-event days had two maxima, one in spring and another one in autumn. The difference in the value of CS between the NPF event and non-event days was the highest in March and the lowest during the summer months.

Figure 5b shows the monthly temperature conditions (T) during the daytime NPF events and non-events. The temperature at which clear-sky NPF events occurred was different for each month. For example, higher temperatures were favorable for NPF during the months when the overall temperature was below 273.15 K (0° C) (months 1, 2, 3, 11 and 12). On the other hand, NPF events tend to occur at lower temperatures when the overall temperature was above 273.15 K (0° C). The highest recorded temperature at which an event occurred during $P > 0.7$ sky was 300 K (25 °C) and the minimum temperature was 252 K (-21 °C). Accordingly, very high or very low temperatures are not favorable conditions for NPF. Although an increase in the ambient temperature results in higher concentrations of monoterpenes due to increased emissions, thereby favoring new particle formation and growth (Kulmala et al., 2004a), Figure 5b shows that very high temperatures tend to suppress NPF. This latter feature is at least partly related to the positive relation between the ambient



temperature and pre-existing aerosol loading (and hence CS) in Hyytiälä (Liao et al., 2014), even though it might also be attributed to the presumable increase in vapor evaporation coefficients, which results in less stable clusters at high temperatures (Paasonen et al., 2012).

The relative humidity (RH) appeared to be lower on NPF event days (9:00-12:00) compared with non-events (9:00-12:00) days (Figure 5c). The RH has a monthly cycle with highest values in winter and lowest ones in summer, opposite to that of T and CS. The difference in RH medians between the NPF events and non-events was the highest in winter and became almost negligible in August. Many speculations have been presented on the effect of high RH on suppressing NPF. For instance, a high RH tends to increase the sinks of aerosol particles and their precursor vapors (CS and coagulation sinks), lowering the NPF probability (Hamed et al., 2011). However, in this study no positive correlation between CS and RH was observed during the clear-sky conditions (Table 1). Previous studies in Hyytiälä proposed that increased RH limits some VOC (Volatile Organic Compounds) ozonolysis reactions, preventing the formation of certain condensable vapors necessary for nucleation (Boy and Kulmala, 2002). We found clear differences in how trace gas concentrations were associated with RH between the NPF event and non-event days (Table 1). For instance, O_3 showed a strong negative correlation with RH during events and non-events. However, while a very strong positive correlation appeared between RH and each of CO , SO_2 and NO_x during non-event days, low or almost no correlation with those during event days. Therefore, it seems plausible that RH affects NPF via atmospheric chemistry rather than via changing the sink term for condensing vapors and small clusters.

After looking at the characteristics of clear-sky NPF event and non-event days in terms of meteorological parameters and CS, we looked at the variation of trace gas (CO , SO_2 , NO_x and O_3) concentrations during these conditions (Figure 6). Out of these gases, at least SO_2 and O_3 are expected to enhance NPF, SO_2 as a precursor for sulfuric acid and O_3 as an oxidant forming ELVOCs (Extremely Low Volatile Organic Compounds) (Donahue et al., 2012; Ehn et al., 2014). However, none of these vapors seemed to have higher concentrations during NPF event days. This suggests that, as tracers of pollution, these gases are strongly linked with high anthropogenic CS, so air masses having high trace gas concentrations often do not result in NPF in Hyytiälä.

3.3 Connection of nucleating precursor vapors with new particle formation rate

3.3.1 Precursor vapor proxies

In this study, we determined $J_{1.5,C}$ using the proxies for both SA and OxOrg. The monthly variations of these precursors (in the time window 9:00-12:00) are shown in the Figure 7. During clear-sky conditions, the SA proxy tended to have the highest median daytime values during the winter months with a maximum in February (Figure 7a). Contrary to this, the seasonal distribution of the SA proxy reported in Hyytiälä appears as double peaks with an absolute maximum in spring and a smaller one in autumn when presenting the data without excluding cloudy days (Nieminen et al., 2014). During winter, both condensation sink and boundary layer height are lower than in the summer (Paasonen et al., 2013), which might explain the higher concentrations of SA during the winter months.

Being a function of temperature, the OxOrg proxy concentration was generally found to follow the monthly cycle of the ambient temperature. The median value of [OxOrg] was higher on NPF events days during every month compared with



non-event days (Figure 7b). The biggest difference in [OxOrg] between the NPF events and non-events, in terms of its median value, was recorded for January and the least difference for May. It is to be noted that the proxy values represent the measured values less accurately during the winter than during the other periods (Kontkanen et al., 2016).

3.3.2 Particle formation rates

The calculated new particle formation rate, $J_{1.5,C}$, approximated with Eq. (5) shows a similar behavior as the OxOrg precursor (see Figures 7 and 8), being higher for the clear-sky NPF event days in comparison with non-event days. Also, the difference in the value of $J_{1.5,C}$ between the NPF events and non-events was the highest in the winter, and the lowest in summer. The monthly cycle of $J_{1.5,C}$ followed closely that of the OxOrg concentration as the latter has higher seasonal variability and is therefore capable of affecting $J_{1.5,C}$ (Figure 8a). Also, the diurnal cycle of $J_{1.5,C}$ during the NPF event days showed an increase along with sunrise, a peak at midday and decrease along with sunset. However, for non-event days the $J_{1.5,C}$ value was relatively constant throughout the day and had clearly lower values than during the NPF event days (Figure 8b).

The formation rate of 3 nm particles is affected not only by the new particle formation rate ($J_{1.5}$) but also by the scavenging of newly-formed particles by coagulation into pre-existing particles. We found that, in general, the values of $J_{3,C}$ calculated using equations (4) and (5) were higher on NPF event days compared with non-event days in all months (Figure 9a). The difference between the event and non-event days was the largest in winter and then decreased towards summer. However, the diurnal cycles of percentiles and medians of $J_{3,C}$ during each month peaked around noon for both NPF events and non-events. One example is presented in Figure 9b, showing that $J_{3,C}$ tended to increase after the sunrise, to peak at about midday and to diminish after sunset. This kind of diurnal cycle was similar for all the months. Hourly values of $J_{3,C}$ calculated during the NPF event days were higher than those during the non-event days. During the spring months, the difference in the media $J_{3,C}$ between the NPF events and non-events, calculated for every half an hour, appeared to increase at about 10:00 and then it started to decrease again at about 13:00 (Figure 9b).

In Figure 10 we present the median diurnal cycles of $J_{3,C}$ plotted against the median diurnal cycles of CS during classified clear-sky NPF events and non-events. The diurnal cycle was calculated by taking the median CS at every half hour throughout the season. On the NPF event days, the CS had higher values during the nighttime and lower values during daytime with a minimum at noon. It is important to remember that J was calculated only for daytime when the SA proxy was available (UV-B radiation is needed for the proxy). On non-event days, the values of CS showed no clear diurnal pattern, had practically no difference between the daytime and nighttime hours, and were roughly twice those recorded during the clear-sky NPF event days. The difference in CS between NPF events and non-events follows from the distinctly different air masses arriving at Hyytiälä. For instance, it has been shown that air-masses originating from the north and passing over Scandinavia have, on average, lower values of CS than the air masses passing over Russia and central Europe (Sogacheva et al., 2005; Nieminen et al., 2015).

On NPF event days, the median approximated formation rate of 3 nm particles had its maximum value at about midday and was significantly higher than that on non-events days (Figure 9b). While a clear negative relation could be seen



between the median seasonal diurnal cycles of CS and $J_{3,C}$ on NPF event days (specifically during daytime), this kind of relation has not been observed during non-event days (Figure 10). Higher values of CS on non-event days is expected, bearing in mind that these particles act as surfaces for scavenging precursor gases and freshly formed particles (Hussein et al., 2008). The association of a high CS with the lower NPF probability has been observed in many studies conducted in Hyytiälä (Boy and Kulmala, 2002; Hyvönen et al., 2005; Baranizadeh et al., 2014) as well as in other rural and urban areas, including Egbert and Toronto in Canada (Jun et al., 2014), Preila in Lithuania (Mordas et al., 2016), Po Valley in Italy (Hamed et al., 2007) and Budapest and K-pusztá in Hungary (Salma et al., 2016).

3.3.3 Threshold separating the NPF events and non-events

Since quite a visible separation could be observed in the calculated values of $J_{3,C}$ between the spring-time clear-sky NPF events and non-events, and since $J_{3,C}$ had its maximum at around midday, the plot of CS versus temperature at midday (11:00-12:00) in spring provides an equation that effectively separates the NPF events from non-events during this season (Figure 11). The equation is calculated using a linear fit that draws a line between the points that separate the maximum number of events data points from the non-events; the data points have been estimated by taking the non-events with the lowest possible CS which still fit the linear separation. More specifically, the days with

$$CS \text{ (s}^{-1}\text{)} > 9.034 \times 10^{-5} \times T \text{ (in Kelvin)} - 0.0213, \text{ (6)}$$

lie above the threshold line and were almost solely non-event days (<2% NPF event days), whereas the days classified as NPF events were mostly below this line. The points above the line were also characterized with higher trace gases concentrations and lower calculated formation rates of 3 nm particles than the rest of the points.

The separation between the clear-sky NPF events and non-events in the CS versus T plot was less evident in autumn and disappeared completely in the summer and winter (Figure 12). Interestingly, yet more than 95% of the NPF event days during these seasons still fell below the threshold line given by Equation 6.

3.3.4 Probability of NPF events and non-events

Since the biggest difference in the calculated 3 nm particle formation rates between the NPF events and non-events was observed around noon (Figure 9b), and since CS and temperature showed promising threshold values for predicting the occurrence of NPF events during spring (up to 98%) (Figure 11), Figure 13 presents the probability of having a NPF event in Hyytiälä at a specific CS and temperature within the time window 11:00-12:00. The probability is calculated taking the fraction of events to the total events and non-events in every cell which is 0.15 steps in CS and 2.5 steps in temperature. The highest probability of having a NPF event corresponded to conditions having moderate temperatures and low values of CS. At high CS levels, there was a zero probability for NPF regardless the temperature. However, at moderate and low values of CS, the probability of having a NPF event decreases as we go to lower temperature. This could be explained by lower emissions of VOCs and thus OxOrg at lower temperatures. Similarly, the probability of NPF decreases as we go to



higher temperatures at constant values of CS. This latter feature might be attributed to conditions unfavorable for clustering due to high temperatures.

4 Conclusion

In this study we combined 20 years of data collected in the SMEAR II station in order to characterize the conditions affecting the frequency of NPF events in that location. By focusing only on clear-sky conditions, we were able to get new insight into differences between the NPF events and non-events. In clear-sky conditions, the meteorological conditions, trace gas concentrations and other studied variables on NPF event days appeared to be similar to those presented in the previous studies which did not consider clear-sky classification. Furthermore, the monthly data refined the analysis so that the differences caused by different quantities became more visible compared the previous studies conducted for this site.

Our results showed that using SA and OxOrg proxies to calculate the apparent formation rates of 1.5 and 3 nm particles works well in differentiating the clear-sky NPF events from non-events. Moreover, during clear-sky conditions the effect of CS on attenuating or even preventing NPF was quite visible: CS was, on average, two times higher on the non-event days compared with the NPF event days. Similarly, many other meteorological variables affected NPF. By using CS and ambient temperature, we were able to find a threshold above which no clear-sky NPF events occurred. This threshold is described with an equation that is able to separate almost 98% of the NPF events from non-events during spring time. In clear sky conditions, when there is plenty of radiation available, NPF events happen as long as the CS is low enough and temperature is moderate. Although a weaker separation was observed in the other seasons, considering only clear-sky conditions enabled us to form a map of the probability of having a NPF event within specific CS and temperature conditions. Using clear-sky conditions appears to bring us one step forward towards understanding NPF and predicting their occurrences in Hyytiälä. Our study serves as a basis to future detailed comparisons with observations to formulate even more robust conclusions.

5 Acknowledgements

This work was supported by the Academy of Finland Centre of Excellence program (grant no. 272041) and Nordic Top-level Research Initiative (TRI) Cryosphere-Atmosphere Interactions in a Changing Arctic Climate (CRAICC). The authors thank the division of atmospheric sciences at the University of Helsinki. We also thank Mrs. Ksenia Tabakova for providing air-mass trajectory data.



6 References

- Aalto, P., Hämeri, K., Becker, E., Weber, R., Salm, J., Mäkelä, J. M., Hoell, C., O'dowd, C. D., Hansson, H.-C., and Väkevä, M.: Physical characterization of aerosol particles during nucleation events, *Tellus B*, 53, 2001.
- Ahlm, L., Liu, S., Day, D. A., Russell, L. M., Weber, R., Gentner, D. R., Goldstein, A. H., DiGangi, J. P., Henry, S. B., and Keutsch, F. N.: Formation and growth of ultrafine particles from secondary sources in Bakersfield, California, *Journal of Geophysical Research: Atmospheres*, 117, 2012.
- Apte, J. S., Marshall, J. D., Cohen, A. J., and Brauer, M.: Addressing global mortality from ambient PM_{2.5}, *Environmental science & technology*, 49, 8057-8066, 2015.
- Asmi, A., Wiedensohler, A., Laj, P., Fjaeraa, A.-M., Sellegri, K., Birmili, W., Weingartner, E., Baltensperger, U., Zdimal, V., and Zikova, N.: Number size distributions and seasonality of submicron particles in Europe 2008–2009, *Atmospheric Chemistry and Physics*, 11, 5505-5538, 2011.
- Baranizadeh, E., Arola, A., Hamed, A., Nieminen, T., Mikkonen, S., Virtanen, A., Kulmala, M., Lehtinen, K., and Laaksonen, A.: The effect of cloudiness on new-particle formation: investigation of radiation levels, *Boreal Environment Research*, 19, 2014.
- Bianchi, F., Tröstl, J., Junninen, H., Frege, C., Henne, S., Hoyle, C., Molteni, U., Herrmann, E., Adamov, A., and Bukowiecki, N.: New particle formation in the free troposphere: A question of chemistry and timing, *Science*, 352, 1109-1112, 2016.
- Boulon, J., Sellegri, K., Venzac, H., Picard, D., Weingartner, E., Wehrle, G., Collaud Coen, M., Bütkofer, R., Flückiger, E., and Baltensperger, U.: New particle formation and ultrafine charged aerosol climatology at a high altitude site in the Alps (Jungfraujoch, 3580 m asl, Switzerland), *Atmospheric Chemistry and Physics*, 10, 9333-9349, 2010.
- Boy, M., and Kulmala, M.: Nucleation events in the continental boundary layer: Influence of physical and meteorological parameters, *Atmospheric Chemistry and Physics*, 2, 1-16, 2002.
- Buenrostro Mazon, S., Riipinen, I., Schultz, D., Valtanen, M., Maso, M. D., Sogacheva, L., Junninen, H., Nieminen, T., Kerminen, V.-M., and Kulmala, M.: Classifying previously undefined days from eleven years of aerosol-particle-size distribution data from the SMEAR II station, Hyttiälä, Finland, *Atmospheric Chemistry and Physics*, 9, 667-676, 2009.
- Buenrostro Mazon, S., Kontkanen, J., Manninen, H. E., Nieminen, T., Kerminen, V.-M., and Kulmala, M.: A long-term comparison of nighttime cluster events and daytime ion formation in a boreal forest, *BOREAL ENVIRONMENT RESEARCH*, 21, 242-261, 2016.
- Bzdek, B. R., Lawler, M. J., Horan, A. J., Pennington, M. R., DePalma, J. W., Zhao, J., Smith, J. N., and Johnston, M. V.: Molecular constraints on particle growth during new particle formation, *Geophysical Research Letters*, 41, 6045-6054, 2014.
- Dal Maso, M., Kulmala, M., Riipinen, I., Wagner, R., Hussein, T., Aalto, P. P., and Lehtinen, K. E.: Formation and growth of fresh atmospheric aerosols: eight years of aerosol size distribution data from SMEAR II, Hyytiälä, Finland, *Boreal Environment Research*, 10, 323, 2005.
- Donahue, N. M., Kroll, J., Pandis, S. N., and Robinson, A. L.: A two-dimensional volatility basis set–Part 2: Diagnostics of organic-aerosol evolution, *Atmospheric Chemistry and Physics*, 12, 615-634, 2012.
- Ehn, M., Thornton, J. A., Kleist, E., Sipilä, M., Junninen, H., Pullinen, I., Springer, M., Rubach, F., Tillmann, R., and Lee, B.: A large source of low-volatility secondary organic aerosol, *Nature*, 506, 476-479, 2014.
- Hallquist, M., Wenger, J., Baltensperger, U., Rudich, Y., Simpson, D., Claeys, M., Dommen, J., Donahue, N., George, C., and Goldstein, A.: The formation, properties and impact of secondary organic aerosol: current and emerging issues, *Atmospheric Chemistry and Physics*, 9, 5155-5236, 2009.
- Hamed, A., Joutsensaari, J., Mikkonen, S., Sogacheva, L., Maso, M. D., Kulmala, M., Cavalli, F., Fuzzi, S., Facchini, M., and Decesari, S.: Nucleation and growth of new particles in Po Valley, Italy, *Atmospheric Chemistry and Physics*, 7, 355-376, 2007.
- Hamed, A., Korhonen, H., Sihto, S. L., Joutsensaari, J., Järvinen, H., Petäjä, T., Arnold, F., Nieminen, T., Kulmala, M., and Smith, J. N.: The role of relative humidity in continental new particle formation, *Journal of Geophysical Research: Atmospheres*, 116, 2011.
- Hari, P., and Kulmala, M.: Station for measuring ecosystem-atmosphere relations, *Boreal Environ. Res*, 10, 315-322, 2005.
- Hussein, T., Martikainen, J., Junninen, H., Sogacheva, L., Wagner, R., Dal Maso, M., Riipinen, I., Aalto, P. P., and Kulmala, M.: Observation of regional new particle formation in the urban atmosphere, *Tellus B*, 60, 509-521, 2008.
- Hyvönen, S., Junninen, H., Laakso, L., Maso, M. D., Grönholm, T., Bonn, B., Keronen, P., Aalto, P., Hiltunen, V., and Pohja, T.: A look at aerosol formation using data mining techniques, *Atmospheric Chemistry and Physics*, 5, 3345-3356, 2005.
- Jun, Y.-S., Jeong, C.-H., Sabaliauskas, K., Leaitch, W. R., and Evans, G. J.: A year-long comparison of particle formation events at paired urban and rural locations, *Atmospheric Pollution Research*, 5, 447-454, 2014.



- 470 Junninen, H., Hulkkonen, M., Riipinen, I., Nieminen, T., Hirsikko, A., Suni, T., Boy, M., LEE, S. H., Vana, M., and Tammet,
471 H.: Observations on nocturnal growth of atmospheric clusters, *Tellus B*, 60, 365-371, 2008.
- 472 Kannosto, J., Lemmetty, M., Virtanen, A., Mäkelä, J., Keskinen, J., Junninen, H., Hussein, T., Aalto, P., and Kulmala, M.:
473 Mode resolved density of atmospheric aerosol particles, *Atmospheric Chemistry and Physics Discussions*, 8, 7263-7288,
474 2008.
- 475 Kerminen, V.-M., and Kulmala, M.: Analytical formulae connecting the “real” and the “apparent” nucleation rate and
476 the nuclei number concentration for atmospheric nucleation events, *Journal of Aerosol Science*, 33, 609-622, 2002.
- 477 Kerminen, V.-M., Petäjä, T., Manninen, H., Paasonen, P., Nieminen, T., Sipilä, M., Junninen, H., Ehn, M., Gagné, S., and
478 Laakso, L.: Atmospheric nucleation: highlights of the EUCAARI project and future directions, *Atmospheric Chemistry and
479 Physics*, 10, 10829-10848, 2010.
- 480 Kerminen, V.-M., Paramonov, M., Anttila, T., Riipinen, I., Fountoukis, C., Korhonen, H., Asmi, E., Laakso, L., Lihavainen,
481 H., and Swietlicki, E.: Cloud condensation nuclei production associated with atmospheric nucleation: a synthesis based
482 on existing literature and new results, *Atmospheric Chemistry and Physics*, 12, 12037-12059, 2012.
- 483 Kirkby, J., Curtius, J., Almeida, J., Dunne, E., Duplissy, J., Ehrhart, S., Franchin, A., Gagné, S., Ickes, L., and Kürten, A.: Role
484 of sulphuric acid, ammonia and galactic cosmic rays in atmospheric aerosol nucleation, *Nature*, 476, 429-433, 2011.
- 485 Kontkanen, J., Järvinen, E., Manninen, H., Lehtipalo, K., Kangasluoma, J., Decesari, S., Gobbi, G., Laaksonen, A., Petäjä,
486 T., and Kulmala, M.: High concentrations of sub-3 nm clusters and frequent new particle formation observed in the Po
487 Valley, Italy, during the PEGASOS 2012 campaign, *Atmospheric Chemistry and Physics Discussions*, 15, 33077-33119,
488 2015.
- 489 Kontkanen, J., Paasonen, P., Aalto, J., Bäck, J., Rantala, P., Petäjä, T., and Kulmala, M.: Simple proxies for estimating the
490 concentrations of monoterpenes and their oxidation products at a boreal forest site, *Atmos. Chem. Phys. Discuss.*, 2016,
491 1-33, 10.5194/acp-2016-477, 2016.
- 492 Kulmala, M., Toivonen, A., Mäkelä, J. M., and Laaksonen, A.: Analysis of the growth of nucleation mode particles
493 observed in Boreal forest, *Tellus B*, 50, 449-462, 1998.
- 494 Kulmala, M., Vehkamäki, H., Petäjä, T., Dal Maso, M., Lauri, A., Kerminen, V.-M., Birmili, W., and McMurry, P. H.:
495 Formation and growth rates of ultrafine atmospheric particles: a review of observations, *Journal of Aerosol Science*, 35,
496 143-176, 2004a.
- 497 Kulmala, M., Suni, T., Lehtinen, K. E. J., Dal Maso, M., Boy, M., Reissell, A., Rannik, Ü., Aalto, P., Keronen, P., Hakola, H.,
498 Bäck, J., Hoffmann, T., Vesala, T., and Hari, P.: A new feedback mechanism linking forests, aerosols, and climate, *Atmos.
499 Chem. Phys.*, 4, 557-562, 10.5194/acp-4-557-2004, 2004b.
- 500 Kulmala, M., Petäjä, T., Nieminen, T., Sipilä, M., Manninen, H. E., Lehtipalo, K., Dal Maso, M., Aalto, P. P., Junninen, H.,
501 and Paasonen, P.: Measurement of the nucleation of atmospheric aerosol particles, *Nature protocols*, 7, 1651-1667,
502 2012.
- 503 Kulmala, M., Kontkanen, J., Junninen, H., Lehtipalo, K., Manninen, H. E., Nieminen, T., Petäjä, T., Sipilä, M.,
504 Schobesberger, S., and Rantala, P.: Direct observations of atmospheric aerosol nucleation, *Science*, 339, 943-946, 2013.
- 505 Kulmala, M., Luoma, K., Virkkula, A., Petäjä, T., Paasonen, P., Kerminen, V.-M., Nie, W., Qi, X., Shen, Y., and Chi, X.: On
506 the mode-segregated aerosol particle number concentration load, *Boreal Environment Research*, 2016.
- 507 Kurtén, T., Torpo, L., Ding, C. G., Vehkamäki, H., Sundberg, M. R., Laasonen, K., and Kulmala, M.: A density functional
508 study on water-sulfuric acid-ammonia clusters and implications for atmospheric cluster formation, *Journal of
509 Geophysical Research: Atmospheres*, 112, 2007.
- 510 Liao, L., Kerminen, V.-M., Boy, M., Kulmala, M., and Dal Maso, M.: Temperature influence on the natural aerosol budget
511 over boreal forests, *Atmospheric Chemistry and Physics*, 14, 8295-8308, 2014.
- 512 Merikanto, J., Spracklen, D., Mann, G., Pickering, S., and Carslaw, K.: Impact of nucleation on global CCN, *Atmospheric
513 Chemistry and Physics*, 9, 8601-8616, 2009.
- 514 Metzger, A., Verheggen, B., Dommen, J., Duplissy, J., Prevot, A. S., Weingartner, E., Riipinen, I., Kulmala, M., Spracklen,
515 D. V., and Carslaw, K. S.: Evidence for the role of organics in aerosol particle formation under atmospheric conditions,
516 *Proceedings of the National Academy of Sciences*, 107, 6646-6651, 2010.
- 517 Mordas, G., Plauškaitė, K., Prokopciuk, N., Dudoitis, V., Bozzetti, C., and Ulevicius, V.: Observation of new particle
518 formation on Curonian Spit located between continental Europe and Scandinavia, *Journal of Aerosol Science*, 2016.
- 519 Nieminen, T., Lehtinen, K., and Kulmala, M.: Sub-10 nm particle growth by vapor condensation—effects of vapor
520 molecule size and particle thermal speed, *Atmospheric Chemistry and Physics*, 10, 9773-9779, 2010.
- 521 Nieminen, T., Asmi, A., Dal Maso, M., Aalto, P. P., Keronen, P., Petäjä, T., Kulmala, M., and Kerminen, V.-M.: Trends in
522 atmospheric new-particle formation: 16 years of observations in a boreal-forest environment, *Boreal Environment
523 Research*, 19, 2014.
- 524 Nieminen, T., Yli-Juuti, T., Manninen, H., Petäjä, T., Kerminen, V.-M., and Kulmala, M.: Technical note: New particle
525 formation event forecasts during PEGASOS–Zeppelin Northern mission 2013 in Hyytiälä, Finland, *Atmospheric
526 Chemistry and Physics*, 15, 12385-12396, 2015.



- Paasonen, P., Nieminen, T., Asmi, E., Manninen, H., Petäjä, T., Plass-Dülmer, C., Flentje, H., Birmili, W., Wiedensohler, A., and Horrak, U.: On the roles of sulphuric acid and low-volatility organic vapours in the initial steps of atmospheric new particle formation, *Atmospheric Chemistry and Physics*, 10, 11223-11242, 2010.
- Paasonen, P., Olenius, T., Kupiainen, O., Kurtén, T., Petäjä, T., Birmili, W., Hamed, A., Hu, M., Huey, L., and Plass-Dümler, C.: On the formation of sulphuric acid-amine clusters in varying atmospheric conditions and its influence on atmospheric new particle formation, *Atmospheric Chemistry and Physics*, 12, 9113-9133, 2012.
- Paasonen, P., Asmi, A., Petäjä, T., Kajos, M. K., Äijälä, M., Junninen, H., Holst, T., Abbatt, J. P., Arneth, A., and Birmili, W.: Warming-induced increase in aerosol number concentration likely to moderate climate change, *Nature Geoscience*, 6, 438-442, 2013.
- Perez, R., Ineichen, P., Seals, R., and Zelenka, A.: Making full use of the clearness index for parameterizing hourly insolation conditions, *Solar Energy*, 45, 111-114, 1990.
- Petäjä, T., Mauldin III, R., Kosciuch, E., McGrath, J., Nieminen, T., Paasonen, P., Boy, M., Adamov, A., Kotiaho, T., and Kulmala, M.: Sulfuric acid and OH concentrations in a boreal forest site, *Atmospheric Chemistry and Physics*, 9, 7435-7448, 2009.
- Petäjä, T., Sipilä, M., Paasonen, P., Nieminen, T., Kurtén, T., Ortega, I. K., Stratmann, F., Vehkamäki, H., Berndt, T., and Kulmala, M.: Experimental observation of strongly bound dimers of sulfuric acid: Application to nucleation in the atmosphere, *Physical review letters*, 106, 228302, 2011.
- Pöschl, U.: Atmospheric aerosols: composition, transformation, climate and health effects, *Angewandte Chemie International Edition*, 44, 7520-7540, 2005.
- Riccobono, F., Schobesberger, S., Scott, C. E., Dommen, J., Ortega, I. K., Rondo, L., Almeida, J., Amorim, A., Bianchi, F., and Breitenlechner, M.: Oxidation products of biogenic emissions contribute to nucleation of atmospheric particles, *Science*, 344, 717-721, 2014.
- Salma, I., Németh, Z., Kerminen, V.-M., Aalto, P., Nieminen, T., Weidinger, T., Molnár, Á., Imre, K., and Kulmala, M.: Regional effect on urban atmospheric nucleation, *Atmospheric Chemistry and Physics*, 16, 8715-8728, 2016.
- Sánchez, G., Serrano, A., and Cancillo, M.: Effect of cloudiness on solar global, solar diffuse and terrestrial downward radiation at Badajoz (Southwestern Spain), *Optica pura y aplicada*, 45, 33-38, 2012.
- Seinfeld, J. H., and Pandis, S. N.: *Atmospheric chemistry and physics: from air pollution to climate change*, John Wiley & Sons, 2012.
- Smith, J. N., Moore, K. F., Eisele, F. L., Voisin, D., Ghimire, A. K., Sakurai, H., and McMurry, P. H.: Chemical composition of atmospheric nanoparticles during nucleation events in Atlanta, *Journal of Geophysical Research: Atmospheres*, 110, 2005.
- Sogacheva, L., Dal Maso, M., Kerminen, V.-M., and Kulmala, M.: Probability of nucleation events and aerosol particle concentration in different air mass types arriving at Hyytiälä, southern Finland, based on back trajectories analysis, *Boreal environment research*, 10, 2005.
- Sogacheva, L., Saukkonen, L., Nilsson, E., Dal Maso, M., Schultz, D. M., De Leeuw, G., and Kulmala, M.: New aerosol particle formation in different synoptic situations at Hyytiälä, southern Finland, *Tellus B*, 60, 485-494, 2008.
- Vakkari, V., Tiitta, P., Jaars, K., Croteau, P., Beukes, J. P., Josipovic, M., Kerminen, V. M., Kulmala, M., Venter, A. D., and Zyl, P. G.: Reevaluating the contribution of sulfuric acid and the origin of organic compounds in atmospheric nanoparticle growth, *Geophysical Research Letters*, 42, 2015.
- Yu, F., Luo, G., Bates, T. S., Anderson, B., Clarke, A., Kapustin, V., Yantosca, R. M., Wang, Y., and Wu, S.: Spatial distributions of particle number concentrations in the global troposphere: Simulations, observations, and implications for nucleation mechanisms, *Journal of Geophysical Research: Atmospheres*, 115, 2010.
- Zhang, R., Khalizov, A., Wang, L., Hu, M., and Xu, W.: Nucleation and growth of nanoparticles in the atmosphere, *Chemical Reviews*, 112, 1957-2011, 2011.



Table 1 Correlation coefficient between different meteorological parameters, gas concentrations and condensation sink (CS) during clear-sky events and non-events during spring (Mar-May, 1996-2015) and time window 9:00 – 12:00. The blue refers to high positive correlation (>0.45), Red refers to high negative correlation (<-0.45).

	CS	T	RH	CO	NO _x	SO ₂	O ₃
	Events						
CS	1	0.28	-0.06	0.33	0.53	0.4	0.23
T	0.28	1	-0.64	-0.37	-0.19	-0.29	0.52
RH	-0.06	-0.64	1	0.26	0.21	0.14	-0.51
CO	0.33	-0.37	0.26	1	0.47	0.36	-0.06
NO_x	0.53	-0.19	0.21	0.47	1	0.58	-0.08
SO₂	0.4	-0.29	0.14	0.36	0.58	1	-0.08
O₃	0.23	0.52	-0.51	-0.06	-0.08	-0.08	1
	Non-Events						
CS	1	0.15	-0.12	0.53	0.34	0.23	0.43
T	0.15	1	-0.81	-0.68	-0.51	-0.55	0.62
RH	-0.12	-0.81	1	0.5	0.45	0.42	-0.64
CO	0.53	-0.68	0.5	1	0.7	0.56	-4.E-04
NO_x	0.34	-0.51	0.45	0.7	1	0.41	-0.07
SO₂	0.23	-0.55	0.42	0.56	0.41	1	-0.13
O₃	0.43	0.62	-0.64	-4E-04	-0.07	-0.13	1



577

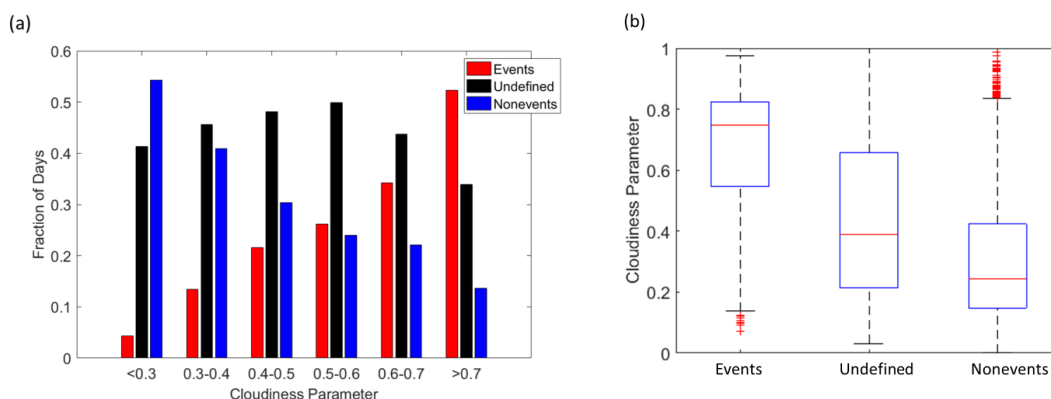


Figure 1: (a) Figure showing the fraction of days which are classified as NPF events, non-events, and undefined days during different sky cloudiness conditions. (b) Cloudiness daily (9:00 – 12:00) medians and percentiles recorded during NPF event, undefined and non-event days. The red line represents the median of the data and the lower and upper edges of the box represent 25th and 75th percentiles of the data respectively. The lines extending 1.5 times from the central box represent the remaining of the data yet still within the relevant statistical limit. The outliers are represented by the red crosses.

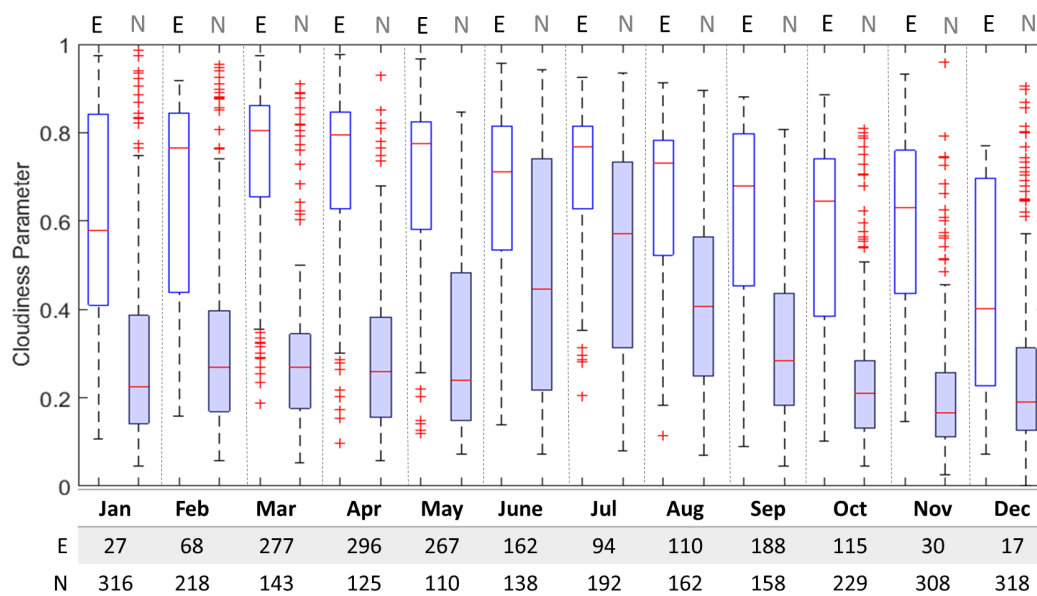


Figure 2: Monthly variation of cloudiness daily (9:00 – 12:00) medians and percentiles recorded during NPF events (E; white) and non-events (N; shaded). Numbers below the plot correspond to the number of data points included in each boxplot. The red line represents the median of the data and the lower and upper edges of the box represent 25th and 75th percentiles of the data respectively. The lines extending 1.5 times from the central box represent the remaining of the data yet still within the relevant statistical limit. The outliers are represented by the red crosses.

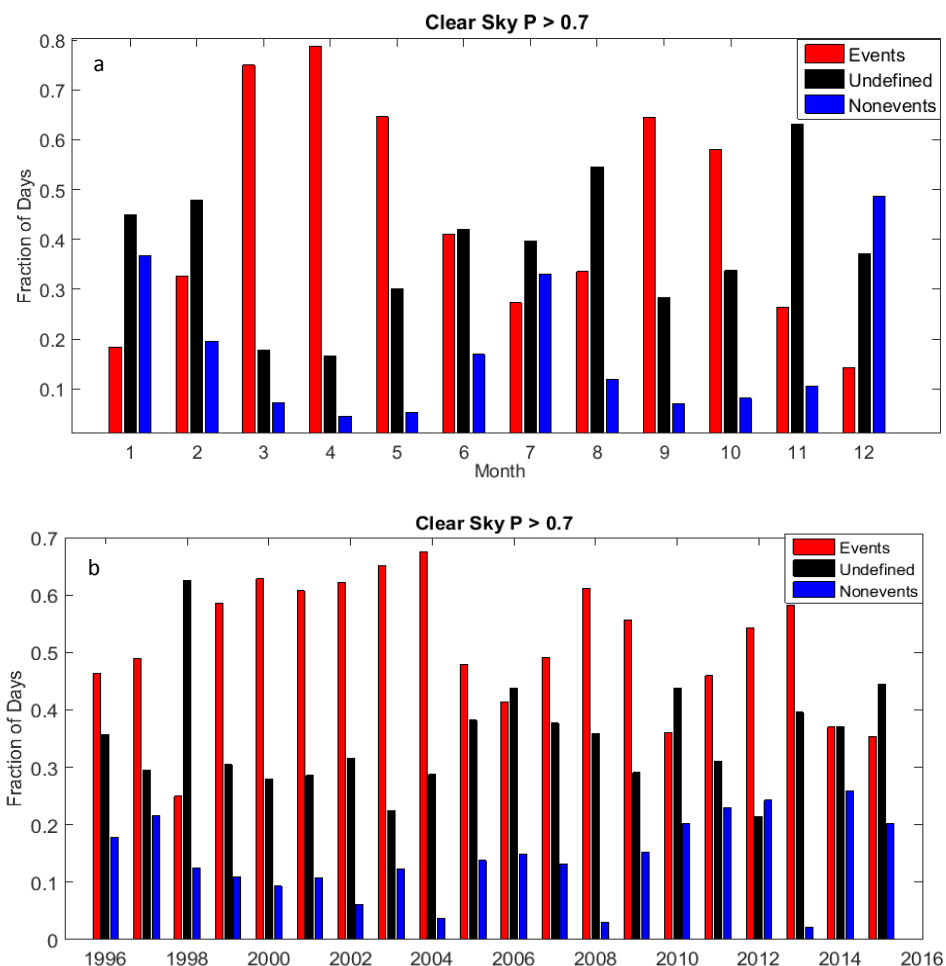


Figure 3: (a) Monthly and (b) yearly fraction of clear-sky days classified as NPF Events, undefined and non-events. In year 1998, global radiation data is limited to 5.4% making the classification bias.

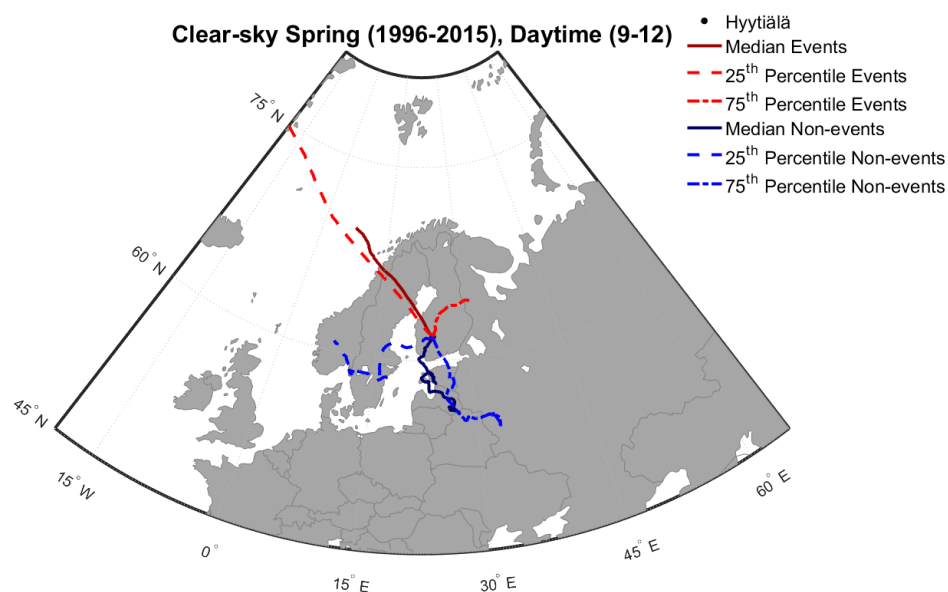
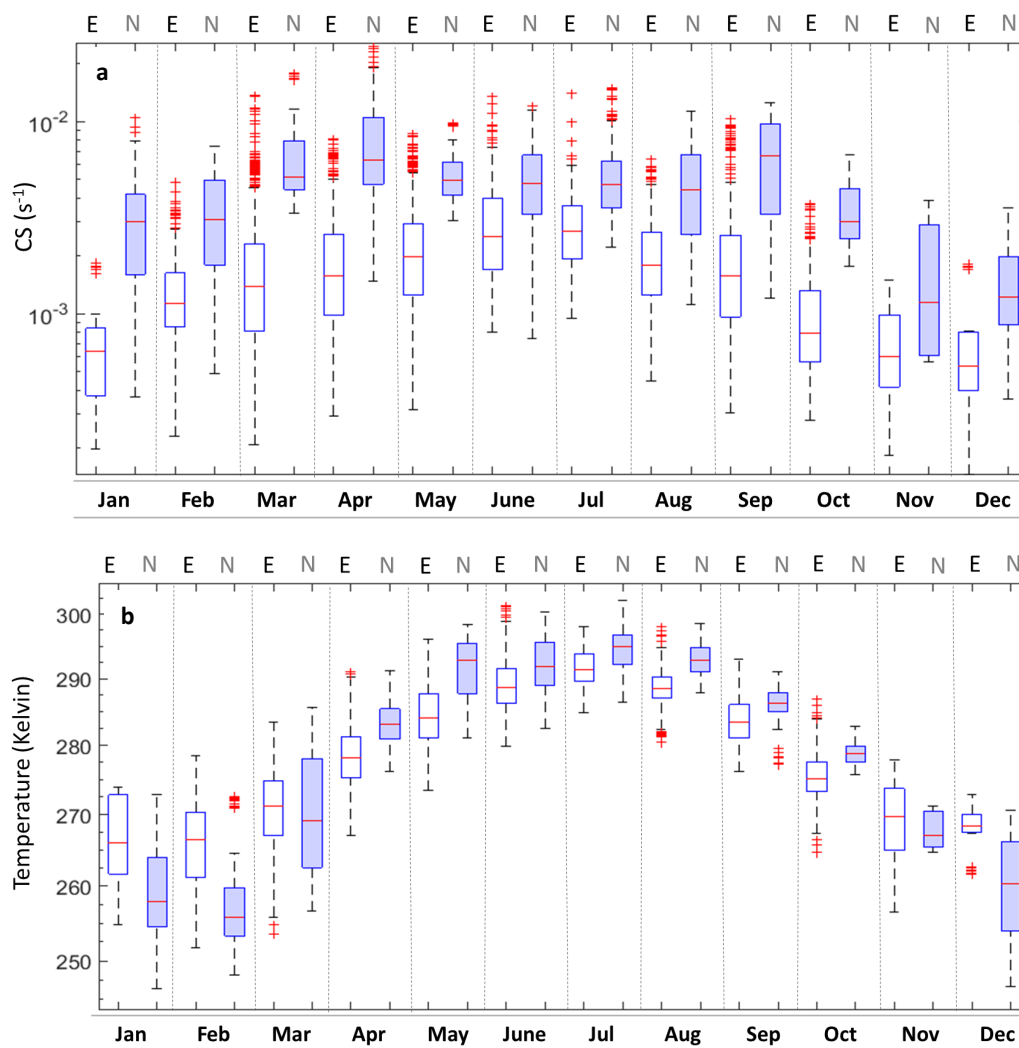


Figure 4: Median and percentiles of 96 hours backward air-mass trajectories arriving to Hyttiälä during spring time (9:00-12:00).



591



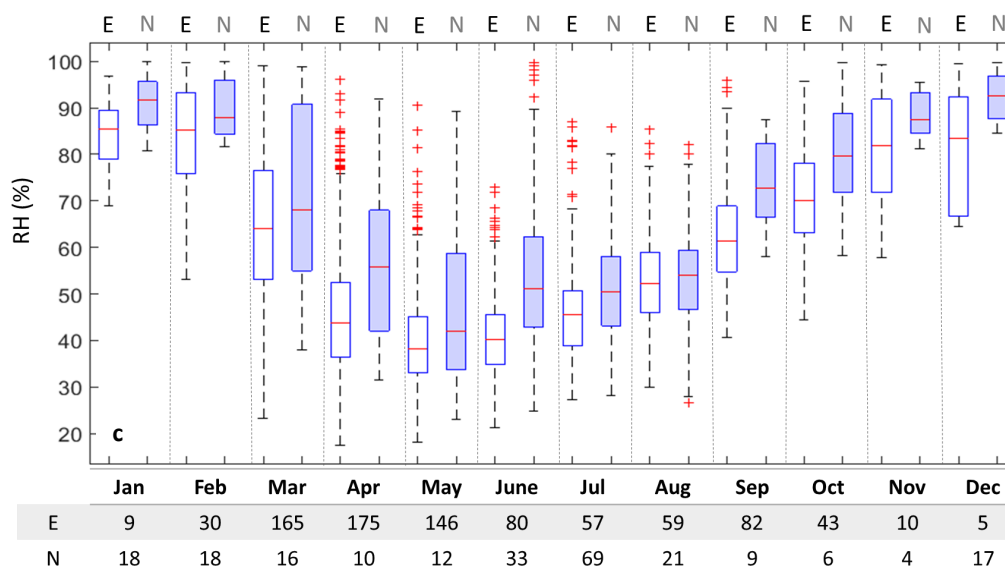


Figure 5: Median and percentiles of monthly variation (9:00 – 12:00) at $P > 0.7$ of (a) CS (b) Temperature and (c) RH during NPF events (E, white) and non-events (N, shaded). The red line represents the median of the data and the lower and upper edges of the box represent 25th and 75th percentiles of the data respectively. The lines extending 1.5 times from the central box represent the remaining of the data yet still within the relevant statistical limit. The outliers are represented by the red crosses.

592

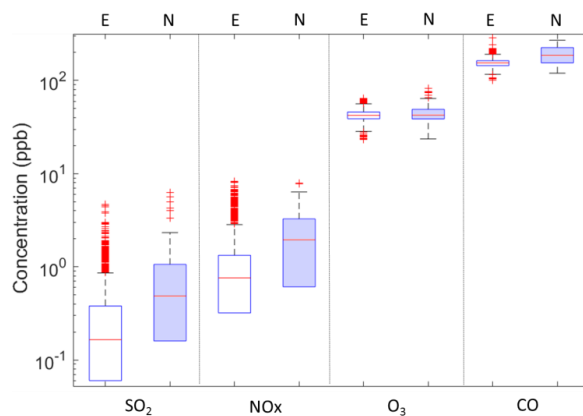


Figure 6: Spring time (months 3,4,5) medians and percentiles of trace gases during clear-sky events (E, white) and non-events (n, shaded) during daytime (9:00 – 12:00). The red line represents the median of the data and the lower and upper edges of the box represent 25th and 75th percentiles of the data respectively. The lines extending 1.5 times from the central box represent the remaining of the data yet still within the relevant statistical limit. The outliers are represented by the red crosses.

593



594

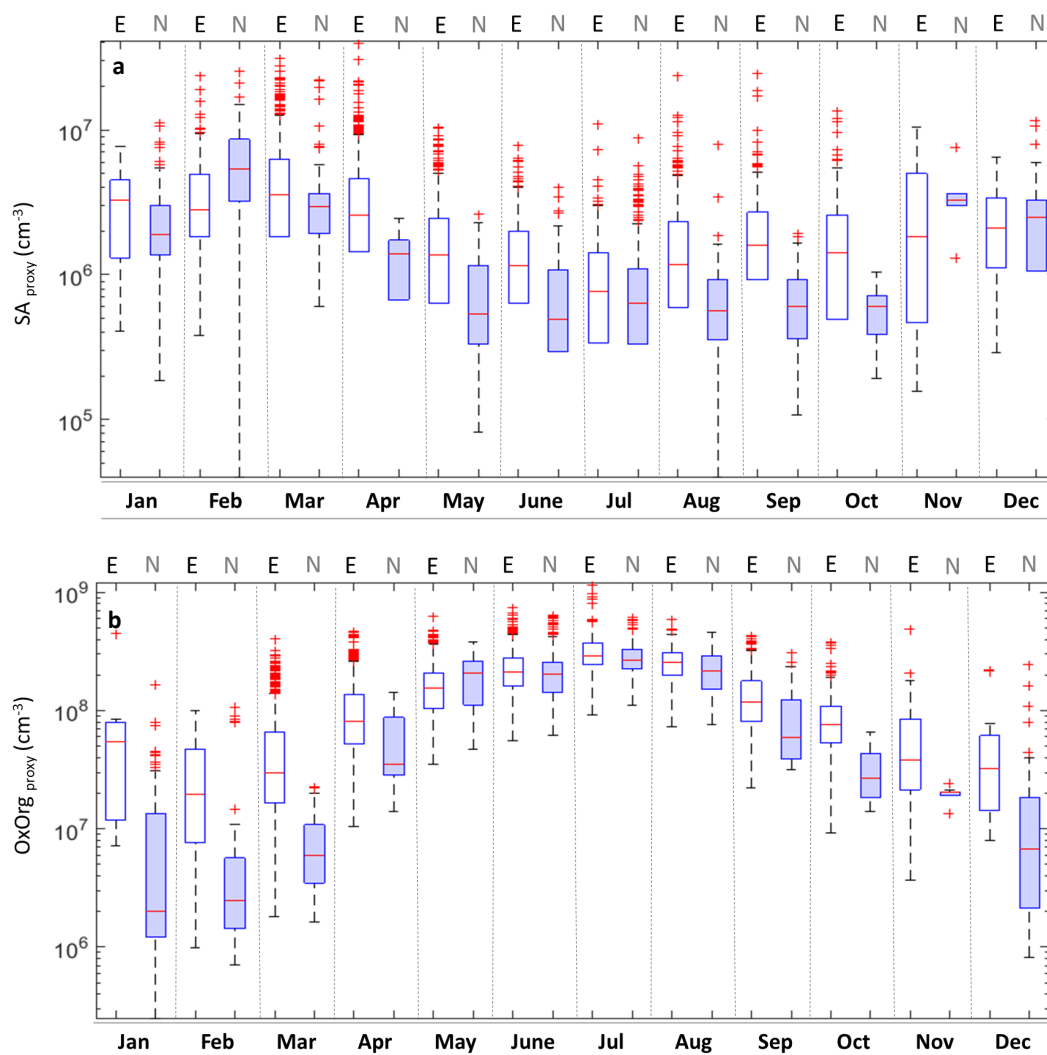


Figure 7: Monthly variation of medians and percentiles of (a) SA proxy and (b) OxOrg proxy at $P > 0.7$ during the time window 9:00 – 12:00 of NPF events (E, white) and non-events (N, shaded). The red line represents the median of the data and the lower and upper edges of the box represent 25th and 75th percentiles of the data respectively. The lines extending 1.5 times from the central box represent the remaining of the data yet still within the relevant statistical limit. The outliers are represented by the red crosses.

595

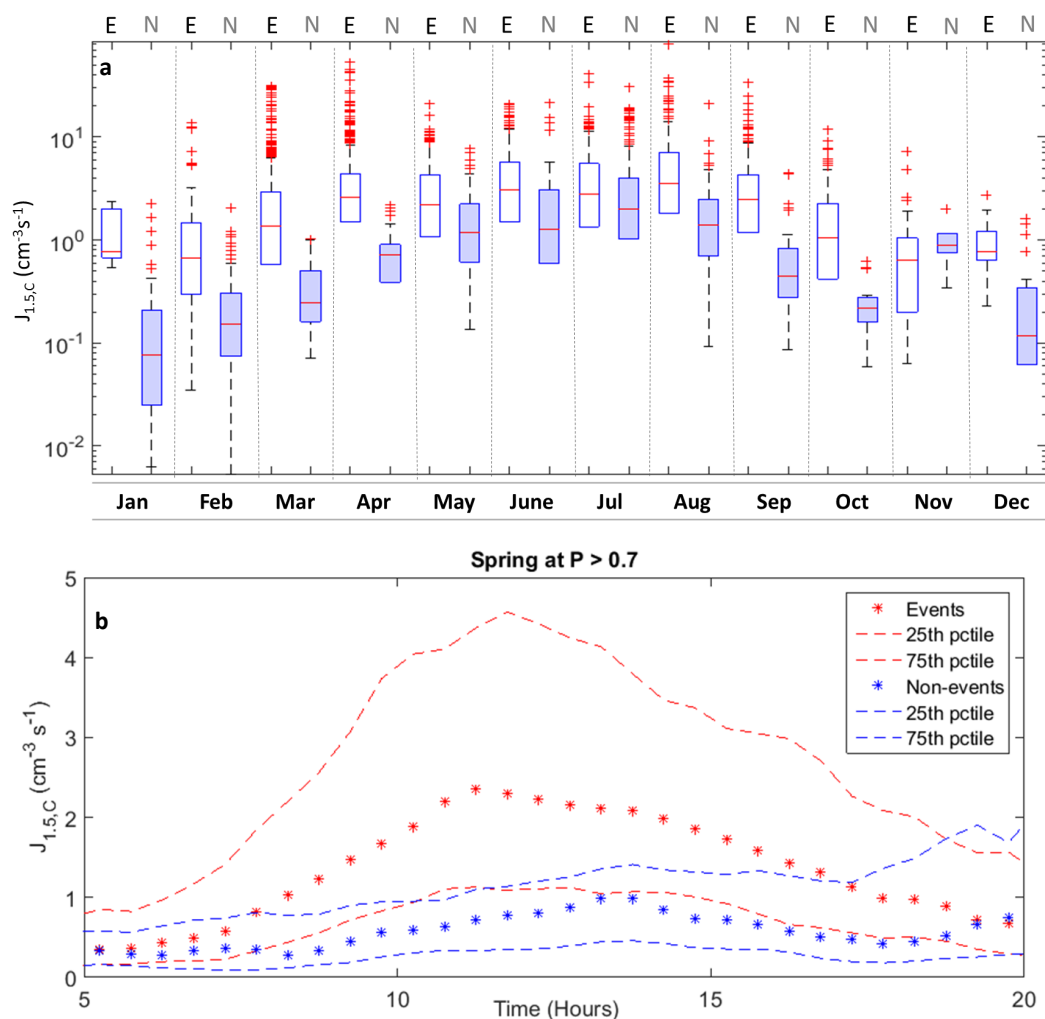
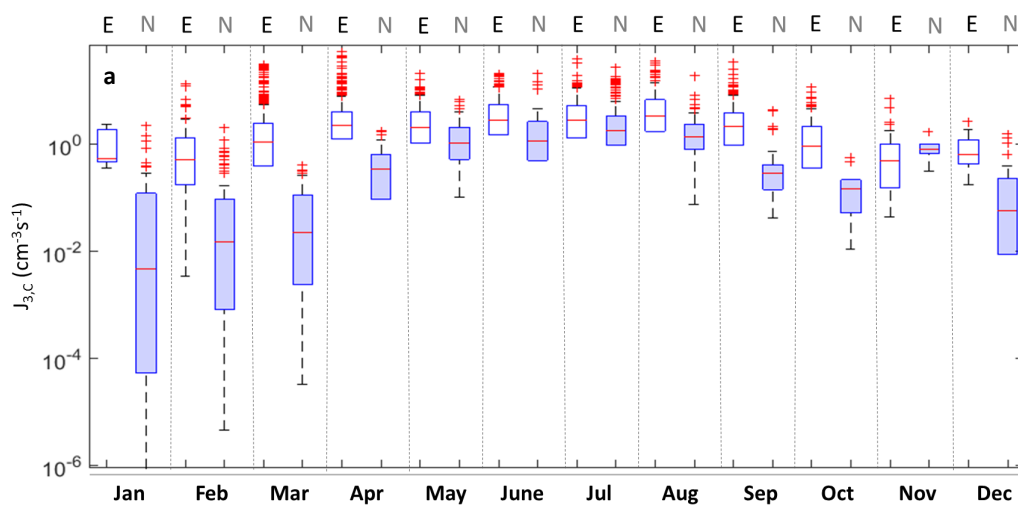
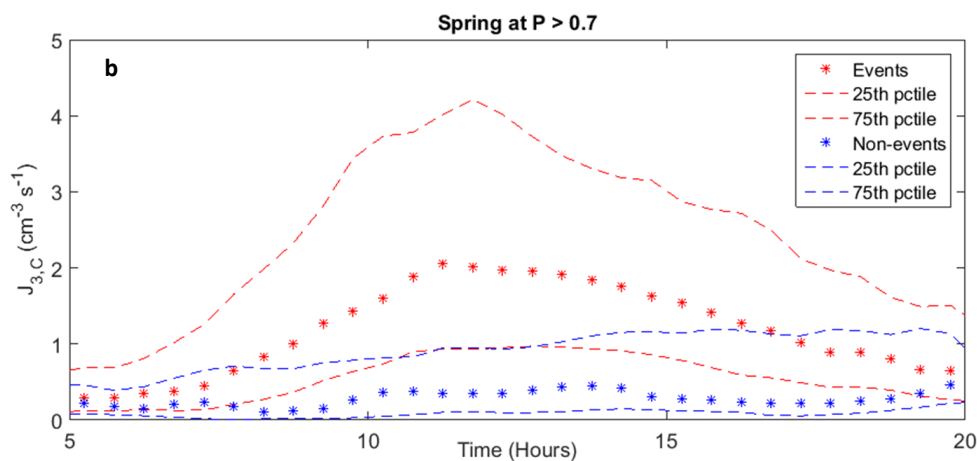


Figure 8: (a) Monthly variation of medians and percentiles of $J_{1.5,C}$ during the time window 9:00 – 12:00 of NPF events (E, white) and non-events (N, shaded). The red line represents the median of the data and the lower and upper edges of the box represent 25th and 75th percentiles of the data respectively. The lines extending 1.5 times from the central box represent the remaining of the data yet still within the relevant statistical limit. The outliers are represented by the red crosses. (b) The diurnal cycle of $J_{1.5,C}$ during Spring. The nighttime is missing in this plot due to unavailable SA proxy which uses UVB to be calculated.



597

598



599

600

601 **Figure 9: (a)** $J_{3,C}$ medians and percentiles during different months separated classified NPF events (E, white) and non-events
 602 (N, shaded) (9:00 -12:00). The red line represents the median of the data and the lower and upper edges of the box represent
 603 25th and 75th percentiles of the data respectively. The lines extending 1.5 times from the central box represent the remaining
 604 of the data yet still within the relevant statistical limit. The outliers are represented by the red crosses (b) The diurnal cycle of
 605 $J_{3,C}$ during spring. The nighttime is missing in this plot due to unavailable SA proxy which uses UVB to be calculated.

606

607

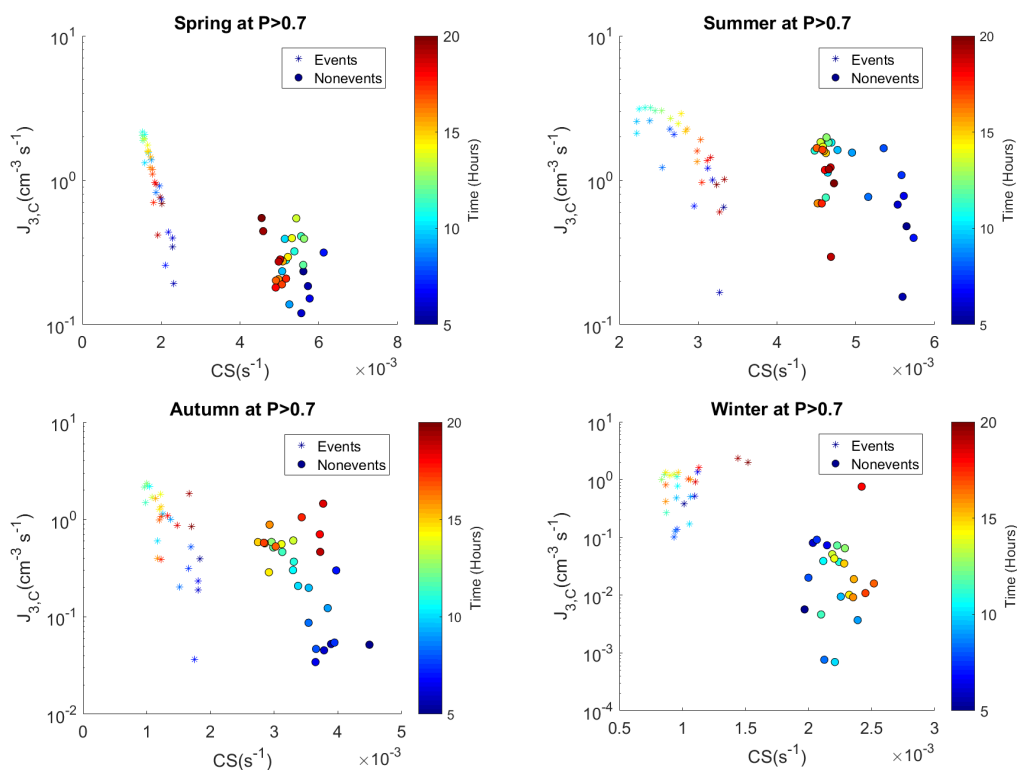


Figure 10: Relationship between seasonal median values of calculated formation rate of 3 nm particles ($J_{3,C}$) and condensation sink (CS) during different times of the day on clear-sky events and non-events.

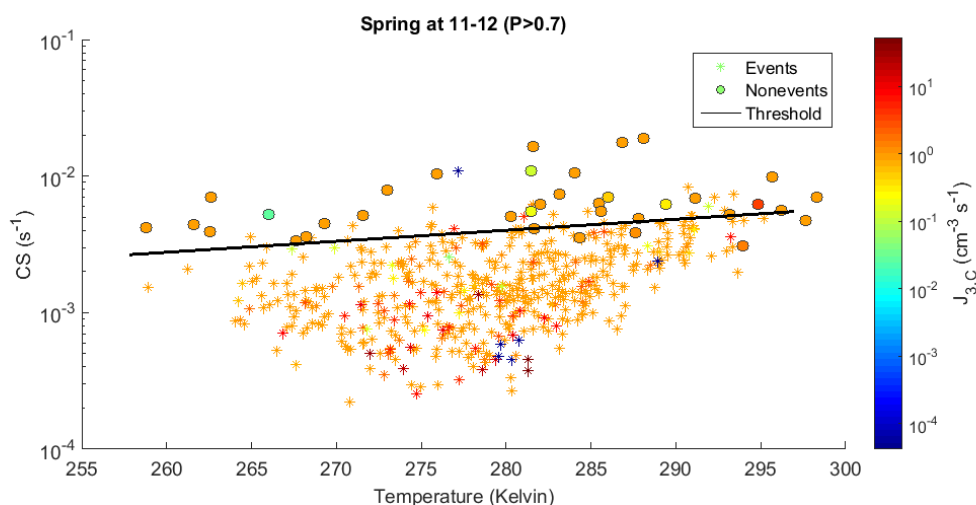


Figure 11: Relationship between temperature and CS during spring time (11:00 – 12:00) NPF clear-sky ($P > 0.7$) event days and non-event days color-coded with $J_{3,C}$. Horizontal line is calculated from equation (6).

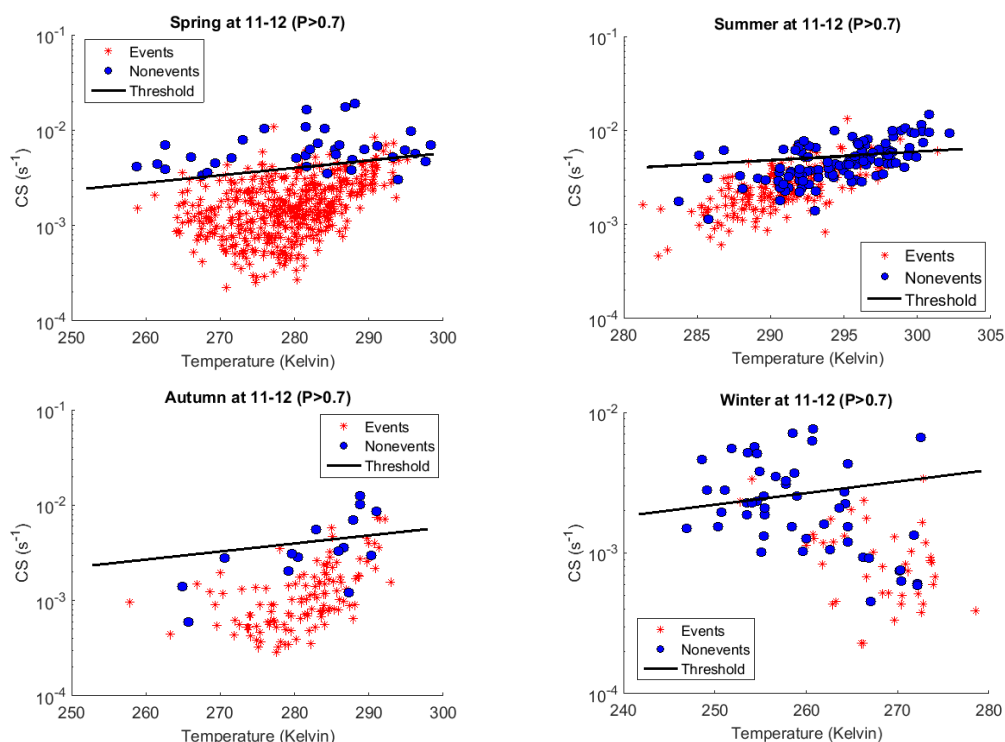


Figure 12: Relationship between CS and Temperature (time window: 11:00 – 12:00) NPF clear-sky event days and non-event days. Horizontal line is calculated via equation (6).

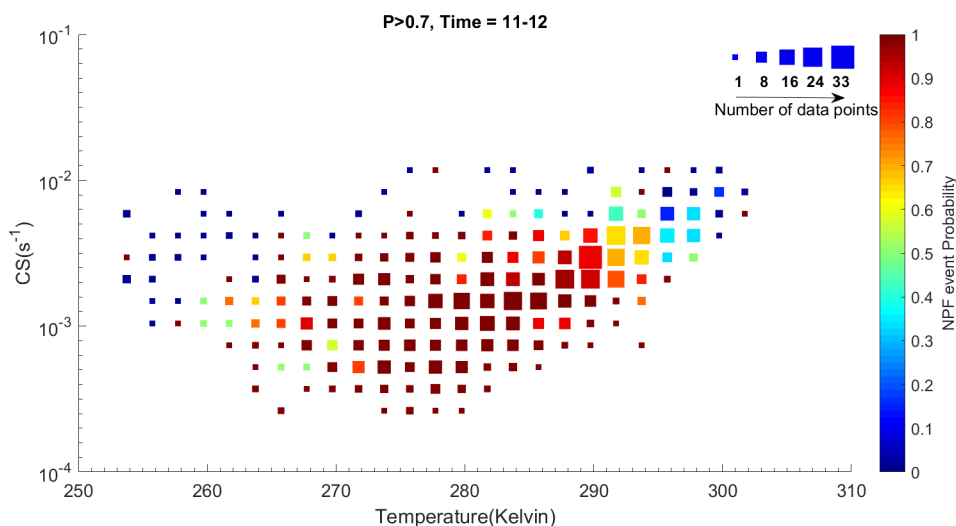


Figure 13: NPF probability distribution based on the CS and temperature conditions during clear-sky days (11:00–12:00). Marker size indicates number of days included in the probability calculation within every cell.